Concentration dependent and independent Si diffusion in ion-implanted GaAs

T. Ahlgren,* J. Likonen,† J. Slotte, J. Räisänen, M. Rajatora, and J. Keinonen

Accelerator Laboratory, University of Helsinki, P.O. Box 43, FIN-00014 Helsinki, Finland

(Received 25 March 1997)

The diffusion of silicon has been studied in $\langle 100 \rangle$ GaAs implanted with 1×10^{16} 40-keV ^{30}Si$^+$ ions/cm^2. The Si concentration profiles were measured by secondary-ion mass spectrometry and nuclear resonance broadening techniques and the defect distributions by the Rutherford backscattering spectrometry channeling technique. The implanted samples were subjected to annealing in argon atmosphere in the temperature range 650 °C–850 °C. Two independent silicon diffusion mechanisms were observed. Concentration independent diffusion, observed as a broadening of the initial implanted distribution, is very slow and is assigned to Si atoms diffusing interstitially. Concentration dependent diffusion with low solubility and extending deep into the sample is quantitatively explained by diffusion via vacancies of Si atoms in the Ga and As sublattices. Diffusion coefficients together with carrier concentration as a function of Si concentration are given at different temperatures. The solid solubility of Si in GaAs has been determined and an exponential temperature dependence observed. An estimate of the amount of Si atoms residing on either Ga or As sites and the amount of Si$_{Ga}^+$-Si$_{As}^-$ pairs is given. Finally, a fast method is presented for solving the diffusion equation numerically. [S0163-1829(97)03331-6]

I. INTRODUCTION

Silicon is the main n-type dopant used in GaAs, and it is usually incorporated into GaAs by ion implantation or by diffusion employing an external source. The diminishing size of the submicrometer devices calls for the use of ion implantation to control the depths and amounts of impurities.[1] Ion implantation is also the only convenient way of introducing impurities exceeding the solid solubility limit; however, ion implantation studies have earlier been done only for concentrations under 10^{17} atoms/cm^3.[2,3] The diffusion of silicon in GaAs utilizing external diffusion sources has been extensively studied over the years. Both Vieland[4] and Antell[5] reported the effect of arsenic pressure on the diffusion rates. Greiner and Gibbons[6] and Kavanagh *et al.*[7] have shown that the diffusion is concentration dependent for high Si concentrations. In the case of low Si concentrations, Schubert *et al.*[8] obtained diffusion coefficients that were concentration independent and two orders of magnitude smaller than those obtained for high Si concentrations by Greiner and Gibbons.[6] Deppe *et al.*[9,10] observed that Si diffusivity is strongly influenced by doping of the GaAs substrate.

Three models have been proposed in the literature to describe concentration dependent Si diffusion in GaAs. Greiner and Gibbons[6] suggested a model in which rapid diffusion takes place when two Si atoms are located on nearest-neighbor Ga and As sites making a neutral donor-acceptor Si$_{Ga}^+$-Si$_{As}^-$ pair. This model is charge neutral and thus independent of the Fermi level; therefore, the diffusion profiles should not depend on the doping of GaAs. However, the experiments of Deppe *et al.*[10] clearly show that the doping species and concentrations have a significant effect on the diffusion profiles of Si atoms.[11] Kavanagh *et al.*[12] proposed a vacancy concentration gradient model. In this model, it is assumed that the vacancies diffuse from the capping layer and substrate interface into the substrate at a finite rate. Under such conditions a nonuniform vacancy distribution is cre-

ated in the surface region. The impurity diffusion therefore becomes dependent on the local vacancy concentration. The third model is the Fermi-level effect model proposed by Yu, Gösele, and Tan,[13] which incorporates the experimental result that Si is an amphoteric impurity. In this model, it is assumed that Si$_{Ga}^+$ and Si$_{As}^-$ diffuse via pairing with Ga and As vacancies, respectively, while the Si$_{Ga}^+$-Si$_{As}^-$ pair does not diffuse. It should be noted that this assumption is just the opposite of that invoked in Greiner's pair diffusion model.

The purpose of this paper is to explain both high and low concentration Si diffusion in GaAs. The solid solubility of substitutional Si in GaAs as a function of temperature is given and the observed exponential behavior is explained qualitatively. The implantation dose used in this study is considerably higher than in earlier studies and the annealings also extend to lower temperatures. By ion implantation, we avoid complicated surface diffusion and the longer annealing times, compared to RTA (rapid thermal annealing), ensure steady-state diffusion. We also present a fast method of calculating the diffusion profiles and use it to fit the theoretical model to the experiments.

II. EXPERIMENT

Commercially prepared samples of undoped, $\langle 100 \rangle$-oriented single-crystal GaAs were implanted by using the 100-kV isotope separator at the University of Helsinki. The 40-keV room-temperature implantations to total fluences of 1×10^{16} ^{30}Si$^+$ atoms/cm^2 were performed in vacuum (10^{-4} Pa), where the $\langle 100 \rangle$ crystal axis was tilted 7° off the beam direction.

The annealings were carried out in a quartz-tube furnace in Ar atmosphere at a pressure of ≈ 660 torr. During the annealings, performed in steps of 50°C, in the temperature interval of 650 °C to 850 °C, the samples were encapsulated by GaAs wafers to minimize impurity buildup on the GaAs surface and the possible loss of arsenic. The annealing tem-

peratures were measured with a calibrated chromel-alumel thermocouple in close contact with the samples.

The ^{1}H$^+$ and ^{4}He$^+$ ion beams used as projectiles in the nuclear resonance broadening (NRB) and Rutherford back-scattering spectrometry (RBS) channeling measurements were generated by a 2.5-MV Van de Graaff accelerator at the University of Helsinki. The concentration profiles of ^{30}Si, measured by the NRB method using the sharp 619.6-keV resonance in the reaction ^{30}Si$(p,\gamma)^{31}$P, were used to normalize the secondary-ion mass spectrometry (SIMS) profiles. The implantation-induced defects were studied by RBS/channeling with 1.5-MeV ^{4}He$^+$ ions. The calculation of the displaced atom distributions was based on the single-scattering double-beam approximation described in detail elsewhere.[14,15] Conventional procedures for NRB and RBS measurements and data analysis were utilized[16] and the stopping powers of Ref. 17 were employed.

The SIMS depth profiling was performed at the Technical Research Center with a double focusing magnetic sector SIMS (VG Ionex IX70S). The 10-keV Cs$^+$ primary ion current was typically 50 nA during depth profiling and the ion beam was raster scanned over an area of 340×370 μm^2. The negative secondary ions ^{30}Si$^-$ and ^{69}Ga$^-$ were monitored during depth profiling. Crater wall effects were avoided by using a 10 % electronic gate and 1-mm optical gate. The pressure inside the analysis chamber was 5×10^{-8} Pa during the analyses. The depth of the craters was measured by a Dektak 3030ST profilometer after SIMS analysis. The uncertainty of the crater depth was estimated to be 5%.

III. DIFFUSION MODEL

A. Diffusion equation

The model outlined below is developed using the procedure of Yu, Gösele, and Tan,[13] which is based on the influence of the Fermi level on Si diffusion. An important assumption in this model is that Si is an amphoteric dopant in GaAs and can occupy either a Ga site or an As site. These substitutional Si atoms then diffuse via Ga and As vacancies. The amount of vacancies depends on the Fermi level, which in turn depends on the silicon concentration. Details of the procedure are given in the Appendix. The results given in the Appendix are used extensively and the reader may refer to it as necessary.

The silicon diffusion rate depends on the vacancy concentration and the migration of the vacancies in the crystal. The present results and the conclusions of Yu, Gösele, and Tan show that for best fits to the experimental data, only vacancies V_{Ga}^0, V_{Ga}^{3-}, and V_{As}^{3-} need to be taken into account, giving the diffusivity of Si atoms in Ga (D_{SG}) and As (D_{SA}) sublattices, respectively

$$D_{SG} = D_{V_{\text{Ga}}^0} \cdot [V_{\text{Ga}}^0] + D_{V_{\text{Ga}}^{3-}} \cdot [V_{\text{Ga}}^{3-}]$$

$$D_{SA} = D_{V_{\text{As}}^{3-}} \cdot [V_{\text{As}}^{3-}], \tag{1}$$

where D is the diffusion constant and the terms in the brackets denote the atomic fractions of the vacancies. The neutral Ga vacancy concentration $[V_{\text{Ga}}^0]$ is unaffected by the Fermi level, while the concentrations of the triply charged Ga and
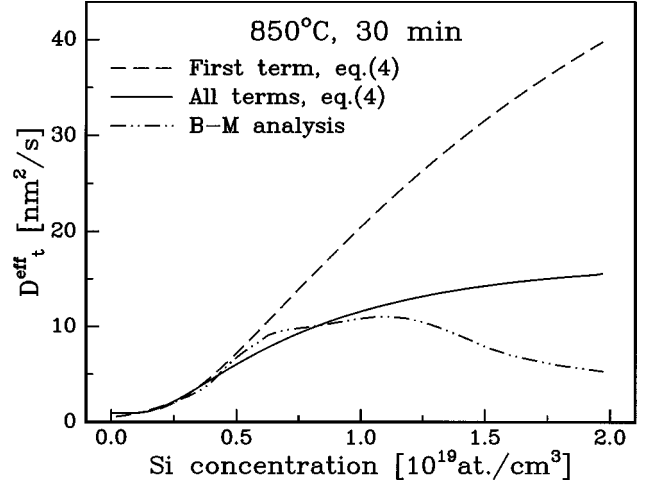

FIG. 1. The effective diffusion coefficient D_t^{eff} as a function of silicon concentration C_t for the 850°C 30-min annealing. Either the first term or all terms in Eq. (4) have been taken into account. Also the result obtained by the Boltzmann-Matano (BM) analysis is presented.

As vacancies change with the Fermi-level position. The extrinsic Si diffusivity becomes[18]

$$D_{SG} = D_{SG}^0 + D_{SG}^{3-} \left(\frac{n}{n_i}\right)^3,$$

$$D_{SA} = D_{SA}^{3-} \left(\frac{n}{n_i}\right)^3, \tag{2}$$

where n_i is the intrinsic and n the extrinsic electron concentration.

The general concentration dependent diffusion equation is

$$\frac{\partial C_t}{\partial t} = \frac{\partial}{\partial x}\left(D(C_t)\frac{\partial C_t}{\partial x}\right), \tag{3}$$

where C_t is the total dopant concentration and $D(C_t)$ is the corresponding diffusion coefficient. From Eq. (2) it may be noted that the diffusivities are functions of electron concentration n, while in the diffusion equation the coefficients depend on the silicon concentration [for the relation between n and C_t, see Eq. (A7) in the Appendix]. The effective diffusion coefficient for the mobile Si$_{\text{Ga}}^+$ and Si$_{\text{As}}^-$ ions diffusing via vacancies becomes

$$D_t^{\text{eff}} = \frac{D_{SG} + \gamma D_{SA}}{1+\gamma} - C_t \frac{(D_{SG} - D_{SA})}{(1+\gamma)^2} \frac{\partial \gamma}{\partial C_t} - \alpha(D_{SG} + D_{SA}), \tag{4}$$

where the electrical compensation ratio[6] γ, $\alpha = dC_p/dC_t$ and Si-pair concentration C_p are defined in the Appendix. Figure 1 presents D_t^{eff} as a function of C_t for the 850 °C, 30-min annealing, where either all terms or only the first term in Eq. (4) have been taken into account. It can be observed that the contribution of the second and third terms is pronounced, contrary to the conclusions of Yu, Gösele, and Tan, where only the first term was taken into account. In the figure, the result obtained by Boltzmann-Matano (BM) analysis[19] is also plotted. The difference between the BM
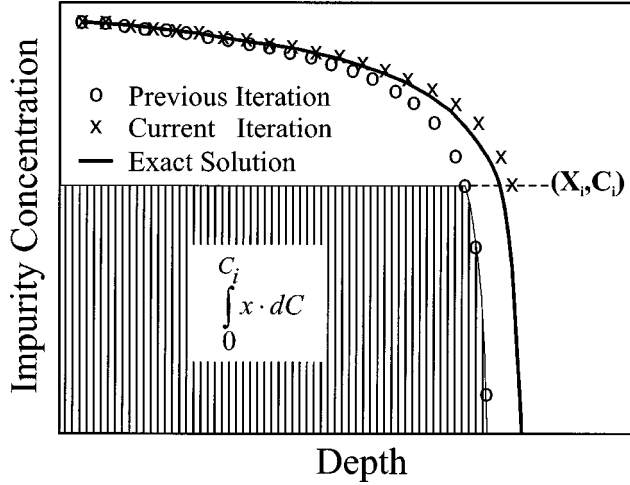
FIG. 2. The plot shows one iteration of a concentration profile. Iterations are stopped when the difference of the x values is within a preset tolerance.
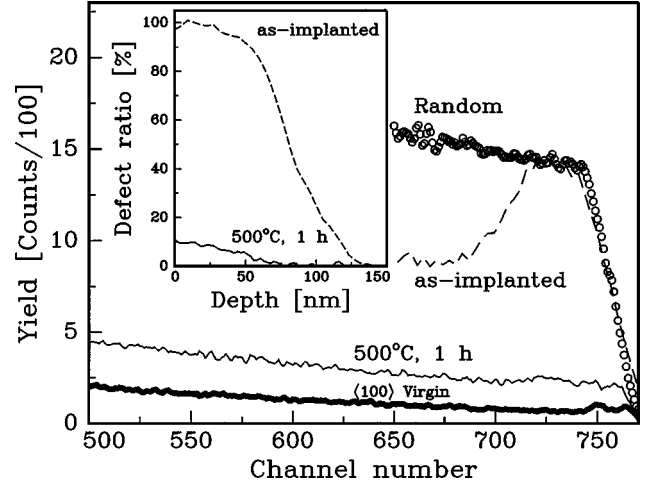

FIG. 3. RBS/channeling spectra for the as-implanted and 500 °C 1-h annealed sample together with the random and $\langle 100 \rangle$ virgin spectra. In the inset are shown the corresponding displaced atom distributions.

analysis and the result given by the diffusion model is here proposed to be because of interstitial atomic diffusion, further discussed in the results. In the present study all terms of Eq. (4) were taken into account.

B. Iteration of the diffusion profile

Solving the diffusion Eq. (3) numerically by the usual flux method is very time consuming. Therefore, we have developed a new method of calculating the depth profiles. By doing the transformation[20] $\eta = x/2\sqrt{t}$, we can rewrite Eq. (3) as an ordinary differential equation

$$-2\eta \frac{dC}{d\eta} = \frac{d}{d\eta}\left(D(C)\frac{dC}{d\eta}\right). \tag{5}$$

By integrating Eq. (5) with respect to η, and taking into account that $D(dC/d\eta) = 0$ when $C = 0$, we obtain

$$-2\int_0^{C_1} \eta dC = \left[D\frac{dC}{d\eta}\right]_{C=0}^{C=C_1} = \left(D\frac{dC}{d\eta}\right)_{C=C_1}. \tag{6}$$

By introducing x and t, replacing the derivative dC/dx by $\Delta C/\Delta x$, and rearranging terms we get

$$\Delta x(C_i) = \frac{-2D(C_i)t\Delta C}{\int_0^{C_i} x dC}. \tag{7}$$

We can now iterate the depth profiles numerically from Eq. (7) by defining a monotonically decreasing vector of concentration values and then calculating the corresponding diffusion constants. By successive iterations of x values, we get a more accurate solution to the diffusion equation, as shown in Fig. 2. The numerical solution of the diffusion equation with this method takes only a few seconds, thus the search for diffusion parameters by least-squares fitting is possible. This method for solving the diffusion equation is well suited for steep diffusion profiles. All of the fitted parameters in the present study have been obtained by this method.

The fitted parameters are the three diffusion coefficients in Eq. (2), the silicon solid solubility in GaAs (C_0), the

vacancy fraction constant (K), and the pairing constant (K_p) defined in the Appendix and the intrinsic carrier concentration (n_i). As a starting point, the concentration and depth values are approximated by the experimental profiles. From these concentration values we calculate the electron concentration n numerically from Eq. (A7), (Appendix), using input values for parameters K and n_i. The n values are used to calculate the effective diffusion coefficient for every concentration using Eqs. (2), (A12), (A15), and (4). The theoretical depth profile may now be calculated employing Eq. (7) and compared with the experimental profile. New parameters are given and the iteration is continued until a satisfactory fit is obtained.

IV. RESULTS AND DISCUSSION

In the present experiments the annealing times are relatively long compared with the heating and cooling times. This makes the diffusion parameters more accurate than those obtained by RTA, which has been employed in most previous studies. It has been shown in many experiments[2,3,12,21,22] that the encapsulant material largely affects the impurity diffusion rate. For samples where the encapsulant functions as a diffusion barrier for As, the Si diffusion proceeds faster due to the high concentration of Ga vacancies. Here we used GaAs wafers as encapsulants to minimize the loss of As from the sample.

The damage induced by ^{30}Si$^+$ ion implantation and annealing of the crystal disorder were studied using RBS/channeling. Figure 3 shows the RBS spectra obtained by 1.5-MeV ^{4}He$^+$ ions for the as-implanted and 500 °C 1-h annealed samples, together with random and $\langle 100 \rangle$ virgin spectra. In the inset, the corresponding displaced atom distributions are shown. For the as-implanted sample, we have a complete loss of crystalline structure to a depth of about 80 nm. It can be noted that already with 1 h annealing at 500 °C, the lattice has recrystallized and the defects annealed. This indicates that the silicon diffusion at depths above 100 nm occurs virtually in a defect-free crystal.

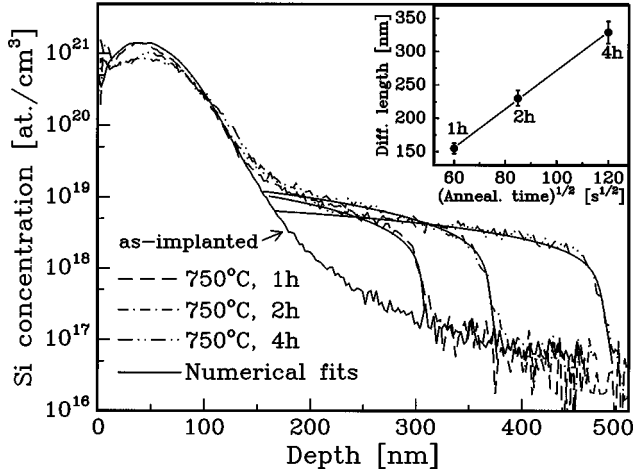Figure 4 shows the results of the SIMS analyses and the

FIG. 4. The SIMS profiles for the as-implanted and 750 °C 1–4-h annealings, together with the fitted profiles. The inset shows the linear dependence of the diffusion length as a function of the square root of the annealing time.

numerical fits for the 1–4-h 750 °C annealings. It can be observed that the diffusion length increases with time and the solid solubility is about 10^{19} atoms/cm^3. The agreement between the experimental profiles and the theoretical fits is good. In the inset the diffusion length is plotted against the square root of the annealing time. The diffusion length is defined here as the depth interval from the beginning of the concentration dependent diffusion region, i.e., at about 160 nm, where the annealed profile starts to deviate markedly from the as-implanted profile, to the end of the profile where the Si concentration has decreased to the background level. The vacancy concentration-gradient model[12] assumes that the vacancy concentration is highest near the surface and decreases into the sample, predicting a depth-dependent diffusion coefficient. This is in contradiction with the result in the inset of Fig. 4, from which it can be observed that the diffusion length is proportional to the square root of the annealing time; i.e., D is not depth dependent.

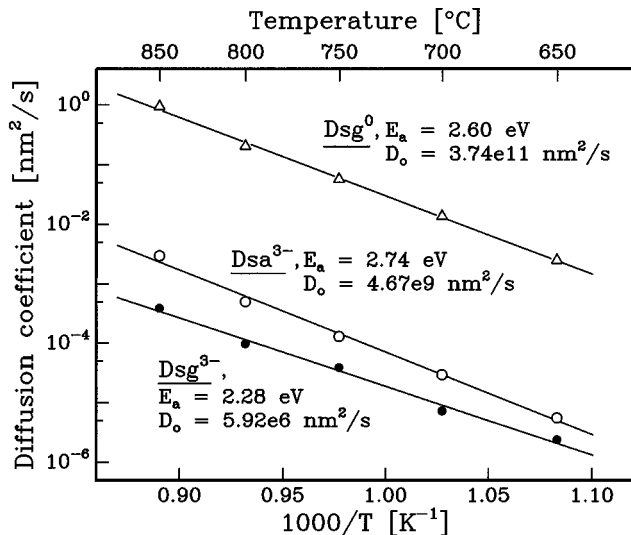

FIG. 5. The Arrhenius plots with the corresponding activation energies and preexponential factors for silicon atom diffusion via gallium and arsene vacancies.
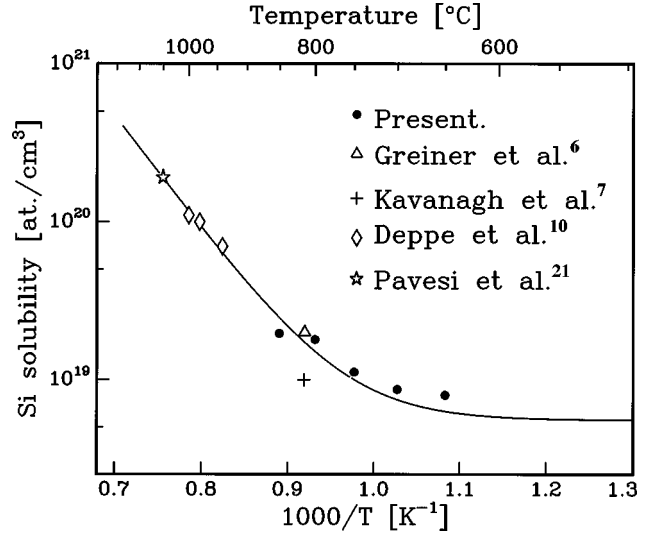

FIG. 6. Substitutional Si solubility in GaAs as a function of temperature.

In Fig. 5 the Arrhenius plots for the intrinsic diffusion coefficients in Eq. (2) are presented. These are well described by the Arrhenius equation $D = D_0 \exp(-E_a/k_b T)$. D_0 is the pre-exponential factor, E_a is the activation energy, and k_B is Boltzmann's constant. Our diffusion coefficients can be compared with results by Yu, Gösele, and Tan,[10] obtained at 815 °C, $D_{SG}^0 \approx 2 \, \text{nm}^2/\text{s}$, $D_{SA}^{3-} \approx 3 \times 10^{-3} \, \text{nm}^2/\text{s}$, and $D_{SG}^{3-} \approx 4 \times 10^{-5} \, \text{nm}^2/\text{s}$. It can be observed that the values for D_{SG}^0 and D_{SA}^{3-} in Ref. 13 are somewhat higher than our values whereas D_{SG}^{3-} is lower. The present activation energies for D_{SG}^0 and D_{SA}^{3-} are in close agreement with those obtained by Yu, Gösele, and Tan. Our calculations give a value of 2.3 eV for the activation energy of D_{SG}^{3-}, which is clearly smaller than the value of ~ 5 eV obtained in that study. Yu, Gösele, and Tan have associated the D_{SG}^{3-} term with Ga self-diffusion in GaAs because this process is characterized by an activation energy of 4–6 eV.[23–26] Theoretical calculations by Chen, Zhang, and Bernholc[27] for Ga self-diffusion are in close agreement with these experimental values. Our result for the activation energy of D_{SG}^{3-} is clearly smaller than that of Ga self-diffusion and thus does not support the idea of linking Si$_{Ga}^+$ diffusion to Ga self-diffusion. Our value for D_{SG}^{3-} is, however, consistent with the activation energy of 2.6 eV obtained for the $(\text{Si}_{Ga}\text{-}V_{Ga})^{2-}$ complex by Chen, Zhang, and Bernholc.[27] They studied also $(\text{Si}_{Ga}\text{-}V_{Ga})^-$ and $(\text{Si}_{Ga}\text{-}V_{Ga})^0$ complexes, but the $(\text{Si}_{Ga}\text{-}V_{Ga})^{2-}$ complex has the lowest formation and migration energies. We also made some calculations using singly charged gallium vacancies, instead of triply charged ones. However, the resulting diffusion fronts were too steep.

Figure 6 shows the present solid solubilities of Si in GaAs together with the literature values,[6,7,10,21] where the solubilities were approximated by extrapolating the Fermi-level-dependent diffusion profiles to zero depth. The solubility is observed to increase exponentially as a function of temperature

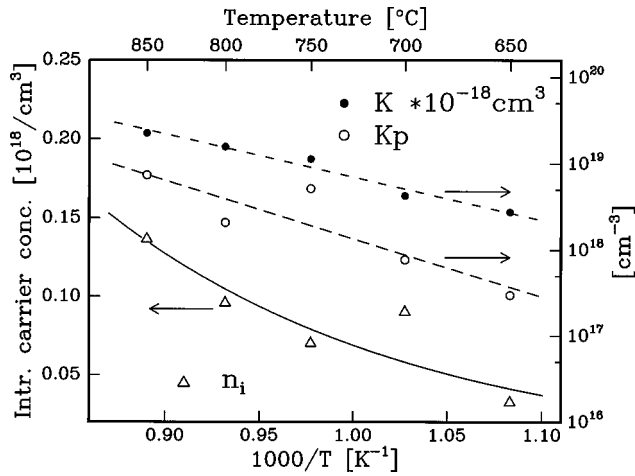$$C_0 = (A + B \times 10^7 e^{C/k_b T}) 10^{18} \text{ atoms/cm}^3, \qquad (8)$$

FIG. 7. The fitting parameters K, Eq. (A3), pairing constant K_p Eq. (A11) and the intrinsic carrier concentration n_i, Eq. (A6) as a function of temperature. The dashed lines are fits and the solid line is drawn to guide the eye.
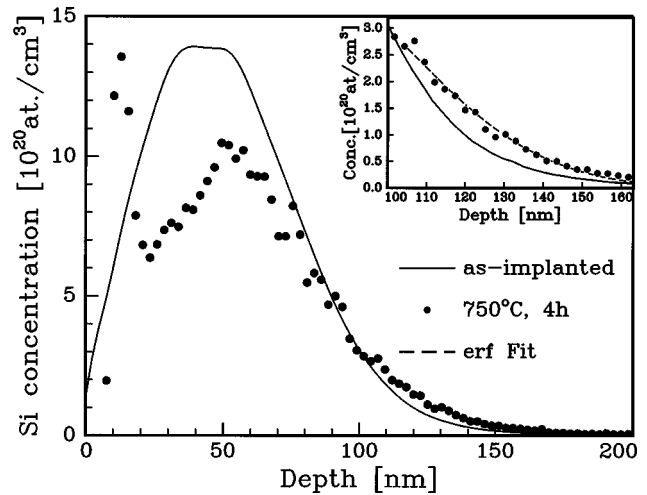

FIG. 8. Error function fitted to the concentration independent diffusion broadening for the 750 °C 4-h annealing. The dots are the values obtained after subtraction of the concentration dependent diffusion fit, as indicated in Fig. 4.

where $A \approx 5.5$, $B \approx 5.7$, and $C \approx -1.44$ eV. This behavior can be explained by the exponential increase of vacancies, $V \propto \exp(-E/kT)$ as a function of temperature, increasing the number of possible substitutional sites Si can occupy.

In Fig. 7, we have plotted the fitting parameters: vacancy fraction constant K, Eq. (A3), the pairing constant K_p, Eq. (A11), and the intrinsic carrier concentration n_i, Eq. (A6) as a function of temperature. Both K parameters exhibit Arrhenius behavior with activation energies of 1.0 eV (for K) and 1.5 eV (for K_p), respectively. The result of Yu, Gösele, and Tan[13] for the parameter K at 815 °C is about 10^{37}/cm^6, which may be compared with the present value of about 2×10^{37}/cm^6. The difference in the activation energies for K obtained in this study and in the work by Yu, Gösele, and Tan ($E_a \approx 1.8$ eV) may be due to the fact that the pairing constant K_p was not included in their calculations. The effect of the pairing constant is a slower diffusion rate increase as a function of Si concentration (see Fig. 1), due to the immobility of the growing number of silicon pairs. Yu, Gösele, and Tan obtained their results by fitting the first term of Eq. (4) to the total Si concentration versus effective diffusion coefficient, $(C_t - D_t^{\text{eff}})$ curve, which was calculated using Boltzmann-Matano analysis. In Fig. 1 are the results from the BM analysis given for the present 850 °C annealing. They explained the decrease of D_t^{eff} at the high C_t end, with the influence of the surface states on the Fermi level being near the GaAs surface. Studying Fig. 4 in more detail, where the 1-4-h annealings at 750 °C are depicted, a broadening of the annealed profiles can be seen in the depth region 110–180 nm. This behavior of the curves cannot be explained by the Fermi-level model. We propose that this broadening is due to slow interstitial Si diffusion, with higher solubility than of substitutional diffusion. To quantify this interstitial diffusion, the contribution of the concentration dependent diffusion was eliminated by subtracting the Fermi-level diffusion fits from the annealed curves. A complementary error function was then fitted to these subtracted curves. The error function is the solution of the solubility limited diffusion equation with a concentration independent diffusion coefficient.[28] An example of such a fit to the 750 °C 4-h

annealing is illustrated in Fig. 8, where the interstitial solubility limit is about 3×10^{20} atoms/cm^3. (The uncertainty of the experimental depths makes the determination of the solubility values difficult.) The interstitial diffusion shows a fairly good Arrhenius behavior with an activation energy of 1.7 eV, as seen in Fig. 9. Based on these calculations it seems that the theoretical diffusion models presented in the literature need the effect of the Si interstitials to be included. The inclusion of interstitials may also resolve the difference between theory and experimental results concerning the existence of V_{As}^{3-} vacancies, which according to theoretical calculations of Baraff and Schlüter[29] do not exist.

Figure 10 presents the theoretical electron concentration given by the present model as a function of the total Si concentration [see Eq. (A7) in the Appendix], for the 650°C, 750 °C, and 850 °C annealings and the experimental data of Gwilliam et al.[30] Gwilliam et al. measured the carrier concentrations of undoped Si implanted GaAs with the
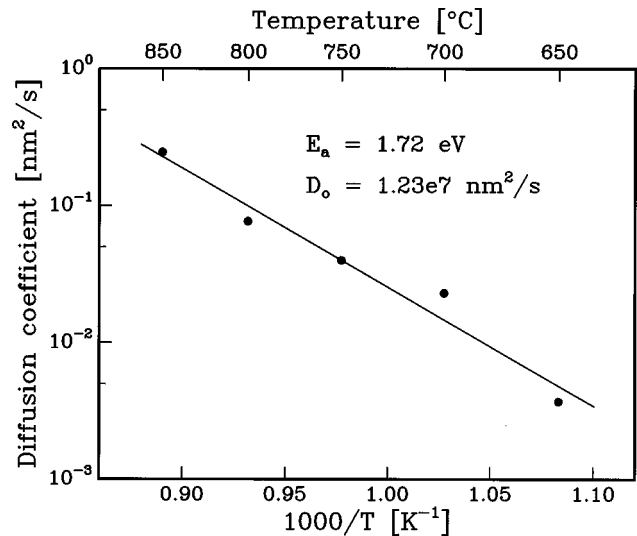

FIG. 9. The Arrhenius plot for the concentration independent silicon diffusion in GaAs.
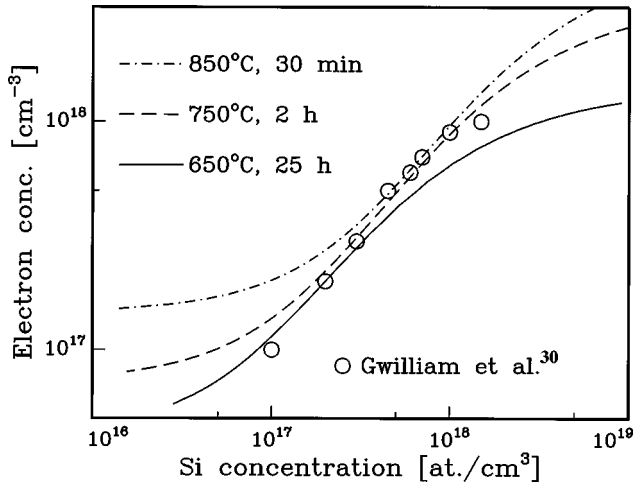
FIG. 10. Theoretical electron concentrations as a function of the total Si concentration. The experimental values of Gwilliam *et al.* have been measured at room temperature after 900 °C, 1000-s annealing.

differential Hall method at room temperature after the 900 °C, 1000-s annealing. Note that theory gives the electron concentrations at the annealing temperature. In the Si concentration region 10^{16}–10^{17} atoms/cm^3, the electron concentration in Fig. 10 increases due to the growing number of intrinsic carriers (n_i), as a function of temperature (see Fig. 7). The electron concentration above 3×10^{17} atoms/cm^3 is approximately independent of the temperature and increases linearly with the Si concentration. This can be understood if we assume that, at room temperature, the silicon and carrier concentrations retain their values frozen-in at the annealing temperature.

The theoretical concentrations of Si atoms on Ga and As sites and the Si-pair concentrations [calculated from Eqs. (A8)–(A13)], are plotted for the 850 °C, 30-min annealing in Fig. 11. It may be noted that the Si atoms occupy only Ga sites at total Si concentrations under 10^{18} atoms/cm^3. This is consistent with the fact that Si acts as a donor in GaAs and
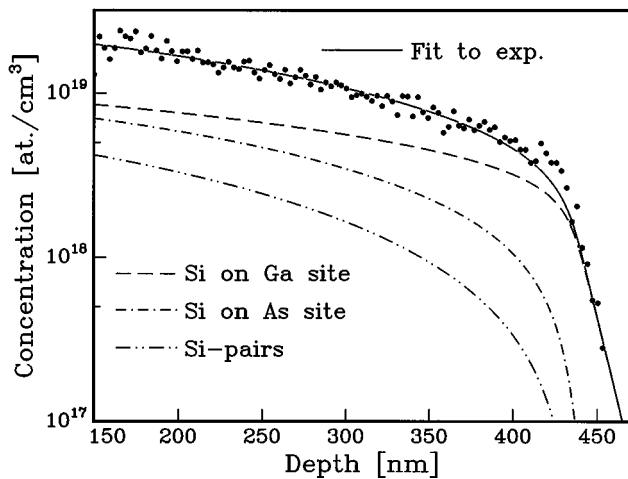

FIG. 11. The theoretical calculations of the lattice locations of the diffused Si atoms for the 850 °C 30-min annealing. At low Si concentrations (the deep end), most of the Si atoms are on Ga sites. For high Si concentrations an increasing fraction of Si atoms take As sites, which also increases the number of Si pairs.

occupies only Ga sites at low concentrations. Above this concentration, the amount of Si atoms occupying As sites and neutral pairs increases faster than the amount of Si atoms on Ga sites.
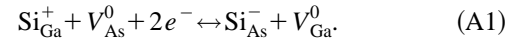
V. CONCLUSIONS

We have studied diffusion of silicon in GaAs implanted at room temperature with 1×10^{16} 40-keV ^{30}Si$^+$ ions/cm^2. The implanted samples were subjected to annealings in argon atmosphere in the temperature range of 650 °C–850 °C. Concentration profiles were measured utilizing SIMS and NRB techniques and implantation-induced defects with RBS/channeling technique. Two independent silicon diffusion mechanisms were observed: (i) the concentration-independent diffusion, which is observed as a broadening of the initial implantation profile, is very slow and is assigned to Si atoms diffusing interstitially; (ii) the concentration-dependent diffusion observed in SIMS profiles is quantitatively explained by diffusion of Si atoms via vacancies in the Ga and As sublattices. This mechanism results from the amphoteric nature of Si and its effect on the Fermi level. Diffusion coefficients, solid solubilities, and carrier concentrations at different annealing temperatures were calculated by improving the model proposed by Yu, Gösele, and Tan. A fast method to solve diffusion equations numerically was developed.

APPENDIX

The simplest chemical reaction describing the change over process between $\mathrm{Si}_{\mathrm{Ga}}^+$ and $\mathrm{Si}_{\mathrm{As}}^+$ is

$$\mathrm{Si}_{\mathrm{Ga}}^+ + V_{\mathrm{As}}^0 + 2e^- \leftrightarrow \mathrm{Si}_{\mathrm{As}}^- + V_{\mathrm{Ga}}^0. \tag{A1}$$

From this reaction we get the relation between the concentrations of $\mathrm{Si}_{\mathrm{Ga}}^+$ and $\mathrm{Si}_{\mathrm{As}}^-$

$$\frac{n^2 C_{SG}}{C_{SA}} = K, \tag{A2}$$

where K is defined as the vacancy fraction constant

$$K = \frac{k[V_{\mathrm{Ga}}^0]}{[V_{\mathrm{As}}^0]}, \tag{A3}$$

where $[V_{\mathrm{As}}^0]$ and $[V_{\mathrm{Ga}}^0]$ are the neutral As and Ga vacancies, respectively, and k is the equilibrium constant for the reaction in Eq. (A1). The total Si concentration (as isolated ions and in $\mathrm{Si}_{\mathrm{Ga}}$-$\mathrm{Si}_{\mathrm{As}}$ pairs) is

$$C_t = C_{SG} + C_{SA}. \tag{A4}$$

For undoped GaAs the charge neutrality condition is

$$n + C_{SA} = p + C_{SG}, \tag{A5}$$

where p presents the hole concentration. For semiconductors the following equation holds

$$np = n_i^2 . \tag{A6}$$

From Eqs. (A2)–(A6) we can write the relation between the total Si concentration C_t and electron concentration n

$$C_t = \frac{(K + n^2)[n - n_i^2/n]}{K - n^2} . \tag{A7}$$

We now assume that in addition to isolated Si_{Ga}^+ and Si_{As}^- ions with concentrations C'_{SG} and C'_{SA}, respectively, also Si_{Ga}-Si_{As} pairs with concentration C_p exist. The total Si concentration can now be written as

$$C_t = C'_{SG} + C'_{SA} + 2 \cdot C_p , \tag{A8}$$

where

$$C'_{SG} = C_{SG} - C_p , \tag{A9}$$

$$C'_{SA} = C_{SA} - C_p . \tag{A10}$$

The concentration of pairs can also be expressed by using the equilibrium reaction between substitutional silicon and silicon existing as pairs

$$C_p K_p = C'_{SG} C'_{SA} , \tag{A11}$$

where K_p is the pair-equilibrium constant. We may now define the electrical compensation ratio as[6]

$$\gamma = \frac{C_{SA}}{C_{SG}} = \frac{n^2}{K} . \tag{A12}$$

The last equality follows from Eq. (A2). The expression for C_p as a function of C_t can be calculated, from previous equations, as

$$C_p = \frac{1}{2} \left\{ (C_t + K_p) - \left[(C_t + K_p)^2 - \frac{4 \gamma C_t^2}{(1 + \gamma)^2} \right]^{1/2} \right\} . \tag{A13}$$

The flux equation for the mobile Si_{Ga}^+ and Si_{As}^- ions, with concentrations C'_{SG} and C'_{SA} is

$$D_t^{\text{eff}} \frac{\partial C_t}{\partial x} = D_{SG} \frac{\partial C'_{SG}}{\partial x} + D_{SA} \frac{\partial C'_{SA}}{\partial x} . \tag{A14}$$

Applying Eqs. (A8)–(A14) an expression for the effective diffusion coefficient may be obtained; see Eq. (4) in Sec. III.
  The derivative needed in the Eq. (4) is

$$\alpha = \frac{\partial C_p}{\partial C_t} = \frac{1}{2} - \frac{1}{4} \left((C_t + K_p)^2 - \frac{4 \gamma C_t^2}{(1 + \gamma)^2} \right)^{-1/2} \left[2(C_t + K_p) \right.$$

$$\left. - \frac{8 \gamma C_t}{(1 + \gamma)^2} - 4 \left(\frac{1}{(1 + \gamma)^2} - \frac{2 \gamma}{(1 + \gamma)^3} \right) C_t^2 \frac{\partial \gamma}{\partial C_t} \right] . \tag{A15}$$

*Author to whom correspondence should be addressed. FAX: +358 9 1918378. Electronic address: tahlgren@beam.helsinki.fi
†Permanent address: Technical Research Center of Finland, Chemical Technology, P.O. Box 1404, FIN-02044 VTT, Finland.
[1] J. C. Zolper, M. Hagerott-Crawford, S. J. Pearton, C. R. Abernathy, and C. B. Vartuli, J. Electron. Mater. **25**, 839 (1996).
[2] J. Kasahara, Y. Kato, M. Arai, and N. Watanabe, J. Electrochem. Soc. **130**, 2275 (1983).
[3] T. Onuma, T. Hariao, and T. Sugawa, J. Electrochem. Soc. **129**, 837 (1982).
[4] L. J. Vieland, J. Phys. Chem. Solids **21**, 318 (1961).
[5] G. R. Antell, Solid-State Electron. **8**, 943 (1965).
[6] M. E. Greiner and J. F. Gibbons, J. Appl. Phys. **57**, 5181 (1985).
[7] K. L. Kavanagh, J. W. Mayer, and C. W. Magee, J. Sheets, J. Tong, and J. M. Woodall, Appl. Phys. Lett. **47**, 1208 (1985).
[8] E. F. Schubert, J. B. Stark, T. H. Chiu, and B. Tell, Appl. Phys. Lett. **53**, 293 (1988).
[9] D. G. Deppe, N. Holonyak, Jr., and J. E. Baker, Appl. Phys. Lett. **52**, 129 (1988).
[10] D. G. Deppe, N. Holonyak, Jr., K. C. Hsieh, P. Gravrilovic, W. Stutius, and J. Williams, Appl. Phys. Lett. **51**, 581 (1987).
[11] D. G. Deppe, N. Holonyak, Jr., F. A. Kish, and J. E. Baker, Appl. Phys. Lett. **50**, 998 (1987).
[12] K. L. Kavanagh, C. W. Magee, J. Sheets, and J. M. Mayer, Appl. Phys. B **64**, 1845 (1988).
[13] S. Yu, U. M. Gösele, and T. Y. Tan, J. Appl. Phys. **66**, 2952 (1989).
[14] J. Keinonen, M. Hautala, E. Rauhala, V. Karttunen, A. Kuronen, J. Räisänen, J. Lahtinen, A. Vehanen, E. Punkka, and P. Hautojärvi, Phys. Rev. B **37**, 8269 (1988).
[15] L. C. Feldman, J. W. Mayer, and S. T. Picraux, *Materials Analysis by Ion Channeling* (Academic, New York, 1982).
[16] K. Nordlund, J. Keinonen, E. Rauhala, and T. Ahlgren, Phys. Rev. B **52**, 15 170 (1995).
[17] M. Rajatora, K. Väkeväinen, T. Ahlgren, E. Rauhala, J. Räisänen, and K. Rakennus, Nucl. Instrum. Methods Phys. Res. B **119**, 457 (1996).
[18] J. W. Mayer and S. S. Lau, *Electronic Materials Science for Integrated Circuits in Si and GaAs* (Macmillan Publishing Company, New York, 1990), p. 209.
[19] J. Crank, *The Mathematics of Diffusion* (Clarendon Press, Oxford, 1975), 2nd ed., p. 231.
[20] L. Boltzmann, Ann. Phys. (Leipzig) **53**, 959 (1894).
[21] L. Pavesi, N. H. Ky, J. D. Ganiére, F. K. Reinhart, N. Baba-Ali, I. Harrison, B. Tuck, and M. Henini, J. Appl. Phys. **71**, 2225 (1992).
[22] S. Matsushita, S. Terada, E. Fujii, D. Inoue, K. Matsumura, and Y. Harada, J. Appl. Phys. **76**, 7300 (1994).
[23] T. Y. Tan and U. Gösele, Appl. Phys. Lett. **52**, 1240 (1988).
[24] M. E. Greiner and J. F. Gibbons, Appl. Phys. Lett. **44**, 750 (1984).
[25] T. Y. Tan and U. Gösele, Mater. Sci. Eng. B **1**, 47 (1988).
[26] T. Y. Tan, H. M. You, S. Yu, U. M. Gösele, W. Jäger, D. W. Boeringer, F. Zypman, R. Tsu, and S.-T. Lee, J. Appl. Phys. **72**, 5206 (1992).
[27] B. Chen, Q.-M. Zhang, and J. Bernholc, Phys. Rev. B **49**, 2985 (1994).
[28] J. Crank, *The Mathematics of Diffusion* (Clarendon Press, Oxford, 1975), 2nd ed., p. 14.
[29] G. A. Baraff and M. Schlüter, Phys. Rev. Lett. **55**, 1327 (1985).
[30] R. Gwilliam, R. Apiwatwaja, R. Wilson, and B. J. Sealy, Nucl. Instrum. Methods Phys. Res. B **106**, 318 (1995).